J. Fluid Mech. (1999), *vol.* 397, *pp.* 45–71. Printed in the United Kingdom

Surface-tension-driven flow in fat fluid wedges and cones

By JOHN BILLINGHAM

Department of Mathematics and Statistics, The University of Birmingham, Edgbaston, Birmingham B15 2TT, UK

(Received 13 January 1999 and in revised form 17 May 1999)

We consider the evolution under the action of surface tension of wedges and cones of viscous fluid whose initial semi-angles are close to $\pi/2$. A short time after the fluid is released from rest, there is an inner region, where surface tension and viscosity dominate, and an outer region, where inertia and viscosity dominate. We also find that the velocity of the tip of the wedge or cone is singular, of $O(\log(1/t))$, as time, t, tends to zero. After a long time, the free surface asymptotes to a similarity form where deformations are of $O(t^{2/3})$, and capillary waves propagate away from the tip. However, a distance of $O(t^{3/4})$ away from the tip, viscosity acts to damp out the capillary waves.

We solve the linearized governing equations using double integral transforms, which we calculate numerically, and use asymptotic techniques to approximate the solutions for small and large times. We also compare the asymptotic solution for the inviscid fat wedge with a numerical solution of the nonlinear inviscid problem for wedges of arbitrary semi-angle.

1. Introduction

Surface-tension-driven flow in a fluid wedge was first analysed by Keller & Miksis (1983) for the case of an inviscid fluid. This analysis has since been generalized to consider pairs of fluid wedges with different densities adjacent to a plane wall (Billingham & King 1995; King, Billingham & Popple 1998). In all of these analyses, the flow of the fluid and deformation of the interface is of similarity form, lengths scaling with $t^{2/3}$. This leads to velocities that scale with $t^{-1/3}$, and hence are singular as $t \to 0$. By examining the order of magnitude of the neglected viscous term in the momentum equation, it is clear that viscosity becomes important for sufficiently small times and cannot be neglected. We should also expect viscosity to act in the far field to damp out the capillary waves that propagate there. In order to examine the effect of viscosity, we study the deformation of a wedge of fluid with semi-angle close to $\pi/2$. In this case, the free surface is initially almost planar and, at leading order as the semi-angle approaches $\pi/2$, we obtain a linear initial/boundary value problem in a half-space. In § 2, we solve this using Fourier–Laplace transforms. We use numerical methods to calculate the free-surface deformation for $t > 0$, and construct asymptotic approximations to the solution for small and large times.

A problem with more practical relevance is the analagous one involving a cone of fluid. When a droplet of fluid detaches from a dripping tap at sufficiently low Reynolds number (Peregrine, Shoker & Symon 1990), the final stage is characterized by the attachment of a slender bridge of fluid to the droplet. After the fluid pinches off, the bridge and the droplet both recoil. The slender bridge then forms a series

of small satellite drops (Keller, King & Ting 1995; Decent & King 1999). We can attempt to model the recoil of the top surface of the droplet by assuming that, at the instant of detachment, it is locally a cone with semi-angle close to $\pi/2$, as suggested by the photographs presented by Peregrine *et al.* (1990). More generally, recent work reviewed by Eggers (1997) has shown that the breakup of fluid droplets and threads is often characterized by the formation of two cones, one slender, one fat. For an inviscid fluid, the fat cone is inverted, with semi-angle approximately 112.8° (Day, Hinch & Lister 1998), whilst for a soap film, treated as a surface-tension-bearing interface between two inviscid regions of gas, the semi-angle is approximately 127° (Chen & Steen 1997). For a sufficiently viscous fluid, the breakup involves the formation of a slender thread (Eggers 1997), but Lister & Stone (1998) have recently shown that the presence of an outer viscous fluid again leads to the formation of a pair of cones. Although we confine our attention here to a single fluid with no outer fluid, we expect that our analysis will give some insight into the behaviour of the fat cone after pinchoff. It is worth noting that, in the literature referred to in this paragraph, the time used to analyse the singularity is the time remaining before pinchoff, whilst in this paper we use the time elapsed since pinchoff. We show in § 3 that, although we must use Hankel–Laplace transforms, the analysis of the problem for the cone is very similar to that for the wedge. However, the results are quantitatively different, with a much smaller deformation of the surface of the cone in the far field. Finally, we note that the cone differs qualitatively from the wedge in that its curvature far from the tip drives a flow in the far field under the assumption that the pressure tends to zero there.

2. The fat wedge

2.1. *Formulation of the initial/boundary value problem*

Consider an initially stationary wedge of incompressible fluid with density ρ, viscosity μ and semi-angle $\pi/2-\tan^{-1}\epsilon$. We take the y-axis along the line of symmetry, pointing into the fluid, and the x-axis perpendicular to this so that the surface of the fluid initially lies at $y = \epsilon|x|$, as illustrated in figure 1(*a*). The surface of the fluid is free and has constant surface tension, γ. At subsequent times $t > 0$, the position of the free surface is given by $y = Y(x,t)$, and the fluid has velocity $\boldsymbol{u}$ and pressure p, as shown in figure 1(*b*).

We can construct length, time, velocity and pressure scales from the physical quantities available in the problem, as

$$l^* = \mu^2/\gamma\rho, \quad t^* = \mu^3/\gamma^2\rho, \quad u^* = \gamma/\mu, \quad p^* = \rho\gamma^2/\mu^2. \tag{2.1}$$

We will neglect the effect of gravity in our analysis. In order to justify this, we can either appeal to an experiment under conditions of microgravity, or under normal conditions of gravity construct the Bond number, $Bo = \rho g l^{*2}/\gamma = g\mu^4/\rho\gamma^3$, which is small if gravity is negligible. For water, with $\gamma \approx 0.07\,\mathrm{kg\,s^{-2}}$, $\rho \approx 10^3\,\mathrm{kg\,m^{-3}}$ and $\mu \approx 10^{-3}\ \mathrm{kg\,m^{-1}\,s^{-1}}$, this gives $l^* \approx 10^{-8}\,\mathrm{m}$, $t^* \approx 2\times10^{-10}\,\mathrm{s}$, $u^* \approx 70\,\mathrm{m\,s^{-1}}$, $p^* \approx 5\times10^6\,\mathrm{Pa}$ and $Bo \approx 3\times10^{-11} \ll 1$. As we shall see below, after a large time, significant deformation of the free surface occurs on the length scale $l^*(t/t^*)^{2/3}$. Gravity will therefore start to become important when $t/t^* = O(Bo^{-3/4}) \approx 8\times10^7$, or $t \approx 0.02$ s. Since l^* is close to the limit of validity of the continuum approximation, we should not expect that the small-time solution that we construct below will be physically relevant for water. However, if we consider a solution of around 85% glycerol in water, such that the viscosity is about 100 times greater than that of pure

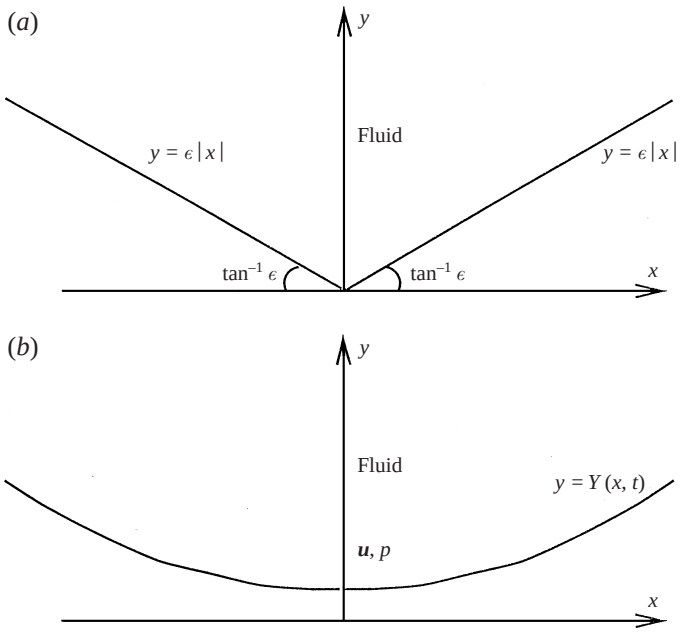

FIGURE 1. The coordinate system and position of the free surface, (*a*) when $t = 0$, (*b*) when $t > 0$.

water, we find that $l^* \approx 10^{-4}\,\mathrm{m}$, $t^* \approx 2 \times 10^{-4}\,\mathrm{s}$, $u^* \approx 0.7\,\mathrm{m\,s^{-1}}$, $p^* \approx 500\,\mathrm{Pa}$ and $Bo \approx 3 \times 10^{-3} \ll 1$. The length scale is far greater than for pure water, and we would expect the features of the small-time solution described below to be experimentally observable. For this fluid, gravity becomes important when $t/t^* \approx 80$.

Suitable dimensionless variables are

$$\hat{x} = x/l^*, \quad \hat{y} = y/l^*, \quad \hat{Y} = Y/l^*, \quad \hat{t} = t/t^*, \quad \hat{\boldsymbol{u}} = \boldsymbol{u}/u^*, \quad \hat{p} = p/p^*, \tag{2.2}$$

in terms of which the initial/boundary value problem becomes

$$\frac{\partial \hat{\boldsymbol{u}}}{\partial \hat{t}} + \hat{\boldsymbol{u}} \cdot \nabla \hat{\boldsymbol{u}} = -\nabla \hat{p} + \nabla^2 \hat{\boldsymbol{u}} \quad \text{for } \hat{y} \geqslant \hat{Y}(\hat{x}, \hat{t}), \tag{2.3}$$

$$\nabla \cdot \hat{\boldsymbol{u}} = 0 \quad \text{for } \hat{y} \geqslant \hat{Y}(\hat{x}, \hat{t}), \tag{2.4}$$

$$\frac{\partial \hat{Y}}{\partial \hat{t}} = \hat{u}_y - \hat{u}_x \frac{\partial \hat{Y}}{\partial \hat{x}} \quad \text{at } \hat{y} = \hat{Y}(\hat{x}, \hat{t}), \tag{2.5}$$

$$\left\{1 - \left(\frac{\partial \hat{Y}}{\partial \hat{x}}\right)^2\right\}\left(\frac{\partial \hat{u}_y}{\partial \hat{x}} + \frac{\partial \hat{u}_x}{\partial \hat{y}}\right) - 4\frac{\partial \hat{Y}}{\partial \hat{x}}\frac{\partial \hat{u}_x}{\partial \hat{x}} = 0 \quad \text{at } \hat{y} = \hat{Y}(\hat{x}, \hat{t}), \tag{2.6}$$

$$-\hat{p} - 2\left\{1 + \left(\frac{\partial \hat{Y}}{\partial \hat{x}}\right)^2\right\}^{-1} \left[\left\{1 - \left(\frac{\partial \hat{Y}}{\partial \hat{x}}\right)^2\right\}\frac{\partial \hat{u}_x}{\partial \hat{x}} + \frac{\partial \hat{Y}}{\partial \hat{x}}\left(\frac{\partial \hat{u}_y}{\partial \hat{x}} + \frac{\partial \hat{u}_x}{\partial \hat{y}}\right)\right] + \frac{\partial^2 \hat{Y}}{\partial \hat{x}^2}\left\{1 + \left(\frac{\partial \hat{Y}}{\partial \hat{x}}\right)^2\right\}^{-3/2} = 0 \quad \text{at } \hat{y} = \hat{Y}(\hat{x}, \hat{t}), \tag{2.7}$$

$$\hat{\boldsymbol{u}} = 0, \quad \hat{Y} = \epsilon|\hat{x}| \quad \text{when } \hat{t} = 0, \tag{2.8}$$

$$\hat{\boldsymbol{u}} \to 0, \quad \hat{p} \to 0 \quad \text{as } \hat{x}^2 + \hat{y}^2 \to \infty, \tag{2.9}$$

$$\hat{Y} = \epsilon|\hat{x}| + o(1) \quad \text{as } \hat{x} \to \infty, \tag{2.10}$$

where $\hat{\boldsymbol{u}} = (\hat{u}_x, \hat{u}_y)$. Note that the only parameter that appears in the problem is ϵ, the initial slope of the interface. We shall restrict our attention to the behaviour when $|\epsilon| \ll 1$, a fat wedge, with $\epsilon < 0$ for an inverted wedge. In this case we expect the deformation of the surface and the subsequent velocity and pressure to remain small, of $O(\epsilon)$. We therefore define new scaled variables to be

$$\hat{x} = \bar{x}, \quad \hat{y} = \bar{y}, \quad \hat{Y} = \epsilon\overline{Y}, \quad \hat{t} = \bar{t}, \quad \hat{\boldsymbol{u}} = \epsilon\bar{\boldsymbol{u}}, \quad \hat{p} = \epsilon\bar{p}. \tag{2.11}$$

At leading order as $\epsilon \to 0$, the initial/boundary value problem becomes

$$\frac{\partial \bar{\boldsymbol{u}}}{\partial \bar{t}} = -\nabla\bar{p} + \nabla^2\bar{\boldsymbol{u}} \quad \text{for } \bar{y} \geqslant 0, \tag{2.12}$$

$$\nabla \cdot \bar{\boldsymbol{u}} = 0 \quad \text{for } \bar{y} \geqslant 0, \tag{2.13}$$

$$\frac{\partial \overline{Y}}{\partial \bar{t}} = \bar{u}_y \quad \text{at } \bar{y} = 0, \tag{2.14}$$

$$\frac{\partial \bar{u}_y}{\partial \bar{x}} + \frac{\partial \bar{u}_x}{\partial \bar{y}} = 0 \quad \text{at } \bar{y} = 0, \tag{2.15}$$

$$-\bar{p} - 2\frac{\partial \bar{u}_x}{\partial \bar{x}} + \frac{\partial^2 \overline{Y}}{\partial \bar{x}^2} = 0 \quad \text{at } \bar{y} = 0, \tag{2.16}$$

$$\bar{\boldsymbol{u}} = 0, \quad \overline{Y} = |\bar{x}| \quad \text{when } \bar{t} = 0, \tag{2.17}$$

$$\bar{\boldsymbol{u}} \to 0 \quad \bar{p} \to 0 \quad \text{as } \bar{x}^2 + \bar{y}^2 \to \infty, \tag{2.18}$$

$$\overline{Y} = |\bar{x}| + o(1) \quad \text{as } \bar{x} \to \infty. \tag{2.19}$$

We now have a linear problem to solve in the half-space $\bar{y} > 0$. Before proceeding, it is convenient to reformulate the problem in terms of a streamfunction, ψ, such that $\bar{u}_x = \partial\psi/\partial\bar{y}$ and $\bar{u}_y = -\partial\psi/\partial\bar{x}$. We also note that (2.12) and (2.13) show that $\nabla^2\bar{p} = 0$. After dropping the overbars on the variables for notational convenience, and now using subscript notation for partial derivatives, for example $\psi_x = \partial\psi/\partial x$, we arrive at

$$\psi_{yt} = -p_x + \psi_{xxy} + \psi_{yyy} \quad \text{for } y \geqslant 0, \tag{2.20}$$

$$p_{xx} + p_{yy} = 0 \quad \text{for } y \geqslant 0, \tag{2.21}$$

$$Y_t = -\psi_x \quad \text{at } y = 0, \tag{2.22}$$

$$\psi_{xx} = \psi_{yy} \quad \text{at } y = 0, \tag{2.23}$$

$$p + 2\psi_{xy} = Y_{xx} \quad \text{at } y = 0, \tag{2.24}$$

$$\psi = 0, \quad Y = |x| \quad \text{when } t = 0, \tag{2.25}$$

$$\psi \to 0, \quad p \to 0 \quad \text{as } x^2 + y^2 \to \infty, \tag{2.26}$$

$$Y = |x| + o(1) \quad \text{as } |x| \to \infty. \tag{2.27}$$

2.2. *The linearized inviscid problem*

Before we proceed to solve the full initial/boundary value problem given by (2.20) to (2.27) it is instructive to consider the inviscid version of the linearized problem. This was first studied by Keller & Miksis (1983) who showed that the solution is of similarity form, lengths scaling with $t^{2/3}$. The linearized version of this problem was

solved by Billingham & King (1995) using Mellin transforms. Note that when the fluid is inviscid (2.20) and (2.24) become

$$\psi_{yt} = -p_x \quad \text{for } y \geqslant 0, \quad \text{and} \quad p = Y_{xx} \quad \text{at } y = 0, \tag{2.28}$$

and we cannot satisfy (2.23), which states that the shear stress vanishes at the free surface. Note that this is a purely hypothetical simplification, since we have seen that there is no dimensionless group whose size indicates that viscosity is negligible. However, we shall show below that the inviscid solution does appear as the leading-order solution of the full problem for $t \gg 1$ in the restricted spatial domain $x \ll t^{3/4}$.

We define the Fourier–Laplace transform of each of the dependent variables as, for example,

$$\tilde{\psi}(\omega, y, s) = \int_0^\infty \mathrm{e}^{-st} \int_{-\infty}^\infty \mathrm{e}^{\mathrm{i}\omega x} \psi(x, y, t) \mathrm{d}x \, \mathrm{d}t, \tag{2.29}$$

with similar definitions for $\tilde{p}$ and $\tilde{Y}$. After applying this double transform, the inviscid problem is reduced to

$$s\tilde{\psi}_y = -\mathrm{i}\omega\tilde{p} \quad \text{for } y \geqslant 0, \tag{2.30}$$

$$\tilde{p}_{yy} - \omega^2\tilde{p} = 0 \quad \text{for } y \geqslant 0, \tag{2.31}$$

$$s\tilde{Y} + \frac{2}{\omega^2} = -\mathrm{i}\omega\tilde{\psi} \quad \text{at } y = 0, \tag{2.32}$$

$$\tilde{p} = -\omega^2\tilde{Y} \quad \text{at } y = 0, \tag{2.33}$$

$$\tilde{\psi} \to 0, \quad \tilde{p} \to 0 \quad \text{as } y \to \infty. \tag{2.34}$$

Note that we have used the fact that, as a generalized function, the Fourier transform of $|x|$ is $-2/\omega^2$ in the sense defined by Lighthill (1958). We can now readily show that

$$\tilde{p} = \frac{2s\mathrm{e}^{-|\omega|y}}{s^2 + |\omega|^3}, \quad \tilde{\psi} = \frac{2\mathrm{i}\omega\mathrm{e}^{-|\omega|y}}{|\omega|(s^2 + |\omega|^3)}, \quad \tilde{Y} = -\frac{2s}{\omega^2(s^2 + |\omega|^3)}. \tag{2.35}$$

We shall confine our attention to the deformation of the interface, whose transform is $\tilde{Y}$. This has simple poles at $s = \pm\mathrm{i}|\omega|^{3/2}$, and a residue calculation allows us to invert the Laplace transform. In combination with the Fourier inversion formula this gives

$$Y(x, t) = -\frac{1}{\pi} \int_{-\infty}^\infty \frac{\mathrm{e}^{-\mathrm{i}\hat{\omega}x}}{\omega^2} \cos(|\omega|^{3/2}t) \, \mathrm{d}\omega. \tag{2.36}$$

If we now write $\xi = x/t^{2/3}$, and change the variable of integration to $\hat{\omega} = t^{2/3}\omega$, we obtain

$$Y(\xi, t) = -\frac{t^{2/3}}{\pi} \int_{-\infty}^\infty \frac{\mathrm{e}^{-\mathrm{i}\hat{\omega}\xi}}{\hat{\omega}^2} \cos|\hat{\omega}|^{3/2} \, \mathrm{d}\hat{\omega}. \tag{2.37}$$

This is only defined as a generalized function, since there is a non-integrable singularity in the integrand at $\hat{\omega} = 0$. However, after subtracting out the transform of the singular part and rewriting as a semi-infinite integral we arrive at the neat formula

$$Y(\xi, t) = t^{2/3}Y_I(\xi) = t^{2/3}\left\{|\xi| + \frac{2}{\pi}\int_0^\infty \frac{\cos\omega\xi\left(1 - \cos\omega^{3/2}\right)}{\omega^2}\mathrm{d}\omega\right\}. \tag{2.38}$$

A simple substitution indicates that our $Y(\xi, t)$ should be equal to $t^{2/3}\{|\xi| + \tilde{y}(\xi)\}$

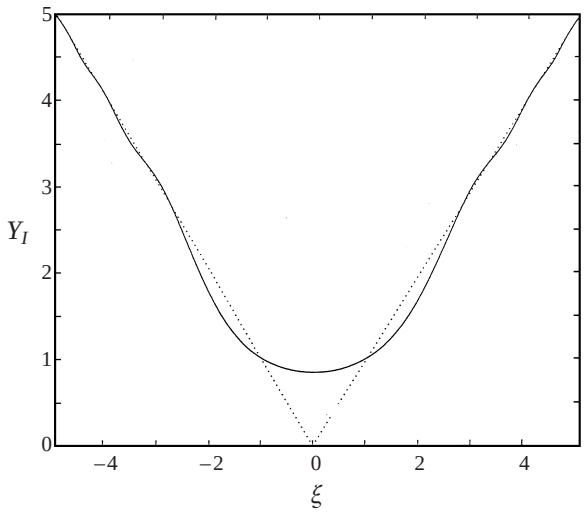

FIGURE 2. The function $Y_I(\xi)$ (solid line) and the initial position of the interface (dotted line).

with $\rho = 0$ in equation (4.46) of Billingham & King (1995). A few manipulations, making use of the results

$$F\left[|x|^{p-1}\right] = \frac{2\Gamma(p)\cos\left(\frac{1}{2}\pi p\right)}{|\omega|^p} \tag{2.39}$$

(Lighthill 1958, p. 43), where $F[.]$ denotes the Fourier transform, and

$$\int_0^\infty \frac{\sin ax}{x^{1-\mu}}\mathrm{d}x = \frac{\Gamma(\mu)}{a^\mu}\sin\left(\tfrac{1}{2}\pi\mu\right) \tag{2.40}$$

(Gradshteyn & Ryzhik 1994, 3.761.4), shows that this is so.

The function $Y_I(\xi)$ can be calculated using Simpson's rule to evaluate the integral in (2.38), and is plotted in figure 2. We can see that the initial singularity in the curvature of the interface is removed by the action of surface tension when $t = 0^+$. The corner of the wedge is blunted and capillary waves propagate on the free surface. The behaviour of these capillary waves for $\xi \gg 1$ was calculated by Billingham & King (1995, Appendix), using manipulations that are far from obvious. Working from (2.37), we can determine the behaviour for $\xi \gg 1$ rather more easily. We first consider the behaviour of the integrand for $|\hat{\omega}| \ll 1$, noting that

$$-\frac{2\cos|\hat{\omega}|^{3/2}}{\hat{\omega}^2} \sim -\frac{2}{\hat{\omega}^2} + |\hat{\omega}| - \frac{1}{12}\hat{\omega}^4 \sim F\left[|\xi| - \frac{1}{\pi\xi^2} + O(\xi^{-5})\right] \quad \text{for } |\hat{\omega}| \ll 1, |\xi| \gg 1. \tag{2.41}$$

There is also a point of stationary phase at $\hat{\omega} = \frac{4}{9}\xi^2$, whose contribution we add to give

$$Y_I = |\xi| - \frac{1}{\pi\xi^2} - \frac{27}{4\pi^{1/2}|\xi|^{7/2}}\sin\left(\frac{4}{27}|\xi|^3 + \frac{\pi}{4}\right) + O(\xi^{-5}) \quad \text{for } |\xi| \gg 1, \tag{2.42}$$

in agreement with (A 10) of Billingham & King (1995).

2.3. *Numerical solution of the nonlinear inviscid problem*

The fully nonlinear inviscid problem, with ϵ not necessarily small, can be solved using a boundary integral method, as described by Billingham & King (1995). We confine our attention in this subsection to positive values of ϵ. Similar results are obtained for $\epsilon < 0$. We define a velocity potential, ϕ, so that $\hat{\boldsymbol{u}} = \nabla\phi$, and ϕ is harmonic in the fluid. We then seek a similarity solution of the form

$$\phi(x, y, t) = t^{1/3}\Phi(\xi, \eta), \quad Y(x, t) = t^{2/3}Y_N(\xi), \tag{2.43}$$

where $\xi = x/t^{2/3}$ and $\eta = y/t^{2/3}$. In terms of these variables we must solve the nonlinear free boundary problem

$$\nabla^2\Phi = 0 \quad \text{for } \eta \geqslant Y_N(\xi), \tag{2.44}$$

subject to

$$\Phi_\eta - \Phi_\xi Y_{N\xi} = \tfrac{2}{3}\left(Y_N - \xi Y_{N\xi}\right) \quad \text{at } \eta = Y_N, \tag{2.45}$$

$$\tfrac{1}{3}\Phi - \tfrac{2}{3}\left(\xi\Phi_\xi + Y_N\Phi_\eta\right) + \tfrac{1}{2}|\nabla\Phi|^2 = -Y_{N\xi\xi}\left(1 + Y_{N\xi}^2\right)^{-2/3} \quad \text{at } \eta = Y_N, \tag{2.46}$$

$$\Phi \to 0 \quad \text{as } \xi^2 + \eta^2 \to \infty, \tag{2.47}$$

$$Y_N = \epsilon|\xi| + o(1) \quad \text{as } |\xi| \to \infty, \tag{2.48}$$

$$Y_{N\xi} = 0 \quad \text{at } \xi = 0. \tag{2.49}$$

Green's integral representation for the harmonic function $\Phi(\xi, \eta)$ in the domain of solution, $D = \{(\xi, \eta) \mid \eta \geqslant Y_N(\xi)\}$, with boundary $\partial D = \{(\xi, \eta) \mid \eta = Y_N(\xi)\}$ is

$$\pi\Phi(\boldsymbol{r}_0) = \int_{\partial D}\left\{\Phi(\boldsymbol{r})\frac{\partial}{\partial n}\ln|\boldsymbol{r} - \boldsymbol{r}_0| - \frac{\partial\Phi}{\partial n}(\boldsymbol{r})\ln|\boldsymbol{r} - \boldsymbol{r}_0|\right\}\mathrm{d}s, \tag{2.50}$$

where

$$\boldsymbol{n} = (Y_N, -1)\,/\left(1 + Y_{N\xi}^2\right)^{1/2} \tag{2.51}$$

is the outward unit normal to D. The kinematic condition (2.45) shows that

$$\frac{\partial\Phi}{\partial n} = -\tfrac{2}{3}\left(\xi Y_{N\xi} - Y_N\right)/\left(1 + Y_{N\xi}^2\right)^{1/2} \tag{2.52}$$

on the boundary, ∂D. Using this in the integral representation (2.50), we can formulate the problem in terms of the value of Φ on ∂D alone, which we denote by

$$\psi(\xi) = \Phi(\xi, Y_N(\xi)). \tag{2.53}$$

By exploiting the symmetry of the flow about $\xi = 0$, we can rewrite (2.50) as

$$\begin{aligned}\pi\psi(\xi_0) = \int_0^\infty \psi(\xi)\Bigg[&\frac{(\xi - \xi_0)Y_N'(\xi) + Y_N(\xi_0) - Y_N(\xi)}{(\xi - \xi_0)^2 + (Y_N(\xi) - Y_N(\xi_0))^2}\\ &+\frac{(\xi + \xi_0)Y_N'(\xi) + Y_N(\xi_0) - Y_N(\xi)}{(\xi + \xi_0)^2 + (Y_N(\xi) - Y_N(\xi_0))^2}\Bigg]\mathrm{d}\xi\\ &+\frac{1}{3}\int_0^\infty (\xi Y_N'(\xi) - Y_N(\xi))\left[\ln\left\{(\xi - \xi_0)^2 + (Y_N(\xi) - Y_N(\xi_0))^2\right\}\right.\\ &\left.+\ln\left\{(\xi + \xi_0)^2 + (Y_N(\xi) - Y_N(\xi_0))^2\right\}\right]\mathrm{d}\xi.\end{aligned} \tag{2.54}$$

By definition

$$\psi'(\xi) = \Phi_\xi + \Phi_\eta Y_N'(\xi), \tag{2.55}$$

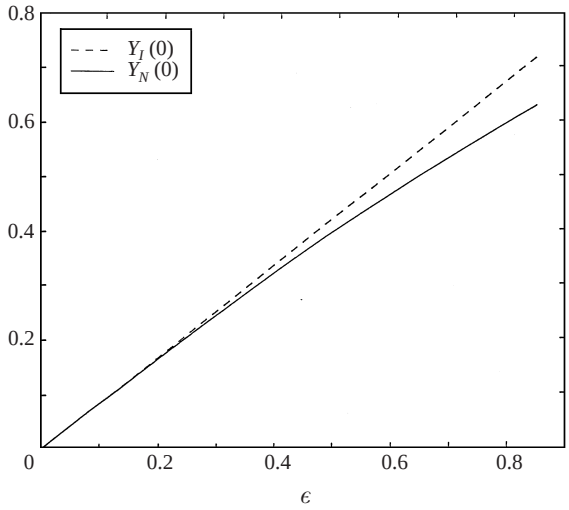

FIGURE 3. The position of the tip of the wedge evaluated both asymptotically, assuming $\epsilon \ll 1$, and numerically, from the full, nonlinear inviscid problem.

which, along with (2.45), leads to

$$\Phi_\xi = \left\{ \tfrac{2}{3} Y_N'(\xi Y_N' - Y_N) + \psi' \right\} / (1 + Y_N'^2), \tag{2.56}$$

$$\Phi_\eta = \left\{ Y_N' \psi' - \tfrac{2}{3} Y_N'(\xi Y_N' - Y_N) \right\} / (1 + Y_N'^2). \tag{2.57}$$

These can be used to rewrite the Bernoulli condition, (2.46), in terms of ψ, which we must solve along with the integral equation (2.54).

We discretize at a set of n equally spaced points $\xi = \xi_i = ih$ for $i = 0, 1, \ldots, n$ and approximate all derivatives with central differences. We truncate the infinite range of the integrals in (2.54) at nh and discretize using a composite trapezium rule. In order to deal with the integrable singularity in (2.54) at $\xi = \xi_0$ we use an analytical integration over the range $\xi_{i-1} \leqslant \xi \leqslant \xi_{i+1}$ that contains the point $\xi = \xi_0$. In this manner we are able to achieve a discretization accurate to $O(h^2)$. Further details are given in Billingham & King (1995). This leads to $2(n-1)$ equations in $2(n+1)$ unknowns. In order to close the discretized system we use the far-field conditions

$$\psi = 0, \quad Y_N = \epsilon \xi_n \quad \text{at } \xi = \xi_n, \tag{2.58}$$

and the symmetry conditions

$$\psi' = 0, \quad Y_N' = 0 \quad \text{at } \xi = 0. \tag{2.59}$$

We solved the resulting $2(n+1)$ nonlinear algebraic equations using the NAG routine C05NBF. This uses a combination of Newtonian iterations and steepest descents. We took $\psi = Y_N = 0$ as our initial guess for the solution with ϵ small. We then used the converged solution as the initial guess for a slightly larger value of ϵ. By continuing in this manner we obtained converged solutions for $0 \leqslant \epsilon \leqslant 0.82$.

Figure 3 shows the position of the tip of the wedge as a function of ϵ, evaluated using both the asymptotic linearized and numerical nonlinear solutions. The difference between the two is less than 4% for ϵ less than about 0.4. Figure 4 makes the comparison over the whole free surface for three values of ϵ.

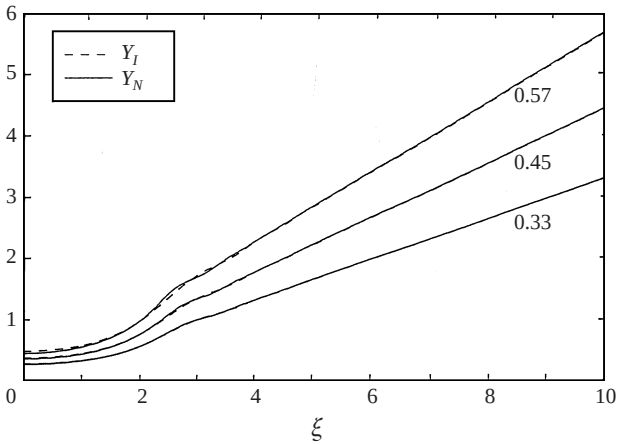

FIGURE 4. The free surface evaluated both asymptotically, assuming $\epsilon \ll 1$, and numerically, from the full, nonlinear inviscid problem, for $\epsilon = 0.33$, 0.45 and 0.57.

2.4. *The full linearized problem*

Turning our attention to the full linearized initial/boundary value problem (2.20) to (2.27), we can define Fourier–Laplace transforms as given before by (2.29) and solve the resulting equations to arrive at

$$\left.\begin{aligned} \tilde{p} &= \frac{2(s+2\omega^2)\mathrm{e}^{-|\omega|y}}{K(\omega,s)}, \\ \tilde{\psi} = \frac{2\mathrm{i}\omega|\omega|}{sK(\omega,s)}\left\{\frac{(s+2\omega^2)\mathrm{e}^{-|\omega|y}}{\omega^2} - 2\mathrm{e}^{-(s+\omega^2)^{1/2}y}\right\}, &\quad \tilde{Y} = \frac{2}{s}\left(\frac{|\omega|}{K(\omega,s)} - \frac{1}{\omega^2}\right), \end{aligned}\right\} \tag{2.60}$$

where

$$K(\omega,s) = (s+2\omega^2)^2 + |\omega|^3\{1 - 4\left(s+\omega^2\right)^{1/2}\}. \tag{2.61}$$

2.4.1. *The deformation of the interface for $t \ll 1$*

Using (2.60) and (2.61) we can write the deformation of the interface as

$$Y(x,t) = \frac{1}{2\pi}\int_{-\infty}^{\infty}\mathrm{e}^{-\mathrm{i}\omega x}\frac{1}{2\pi\mathrm{i}}\int_{c-\mathrm{i}\infty}^{c+\mathrm{i}\infty}\frac{2\mathrm{e}^{\sigma}}{\sigma} \times\left\{\frac{|\omega|}{\left(t^{-1}\sigma+2\omega^2\right)^2 + |\omega|^3 - 4|\omega|^3\left(t^{-1}\sigma+\omega^2\right)^{1/2}} - \frac{1}{\omega^2}\right\}\mathrm{d}\sigma\,\mathrm{d}\omega, \tag{2.62}$$

where c is real and takes the Laplace inversion contour to the right of any singularities in the integrand. We have also made the change of variable $\sigma = st$. We can obtain the behaviour of Y for $x = O(1)$ by expanding the integrand for $t \ll 1$ so that

$$Y(x,t) \sim \frac{1}{2\pi}\int_{-\infty}^{\infty}\mathrm{e}^{-\mathrm{i}\omega x}\frac{1}{2\pi\mathrm{i}}\int_{c-\mathrm{i}\infty}^{c+\mathrm{i}\infty}\frac{2\mathrm{e}^{\sigma}}{\sigma} \times\left(-\frac{1}{\omega^2} + t^2\frac{|\omega|}{\sigma^2} - 4t^3\frac{|\omega|^3}{\sigma^3}\right)\mathrm{d}\sigma\,\mathrm{d}\omega \quad \text{as } t \to 0 \text{ for } x = O(1). \tag{2.63}$$

Evaluating these inverse Fourier transforms of generalized functions leads to

$$Y(x,t) \sim |x| - \frac{t^2}{\pi x^2} - \frac{2t^3}{\pi x^4} \quad \text{as } t \to 0 \quad \text{for } x = O(1). \tag{2.64}$$

The first two terms are the same as those that appear in the far-field expansion of the inviscid solution, (2.42). They indicate that the expansion becomes non-uniform when $x = O(t^{2/3})$. The third term is due to the effect of viscosity and leads to an earlier non-uniformity, between the second and third terms when $x = O(t^{1/2})$.

We can examine the deformation of the interface when $x = O(t^{1/2})$ by defining $x = t^{1/2}\hat{x}$, $\omega = t^{-1/2}\hat{\omega}$, in terms of which (2.62) gives

$$Y(\hat{x},t) \sim t^{1/2}|\hat{x}| + \frac{t}{2\pi}\int_{-\infty}^{\infty} \mathrm{e}^{-\mathrm{i}\hat{\omega}\hat{x}} \frac{1}{2\pi\mathrm{i}} \int_{c-\mathrm{i}\infty}^{c+\mathrm{i}\infty} \frac{2\mathrm{e}^{\sigma}}{\sigma} \times \left\{ \frac{|\hat{\omega}|}{\left(\sigma + 2\hat{\omega}^2\right)^2 - 4|\hat{\omega}|^3\left(\sigma+\hat{\omega}^2\right)^{1/2}} \right\} \mathrm{d}\sigma\, \mathrm{d}\hat{\omega} \quad \text{as } t \to 0 \text{ for } \hat{x} = O(1). \tag{2.65}$$

It is now tempting to define a new variable $\hat{\sigma} = \sigma\hat{\omega}^{-2}$ in order to simplify this double integral. However, since $\hat{\omega}$ passes through zero this is not possible. Note that the integrand is of $O(|\hat{\omega}|^{-1})$ as $|\hat{\omega}| \to \infty$, so the inverse Fourier transform only exists as a generalized function. In order to reformulate (2.65) in terms of ordinary functions, so that the inversion integral can be evaluated, we first note that

$$F^{-1}\left[\frac{1}{|\hat{\omega}|}\right] = -\frac{1}{\pi}\log|\hat{x}| + C(t), \qquad F\left[-\frac{1}{\pi}\log|\hat{x}|\right] = \frac{1}{|\hat{\omega}|}, \tag{2.66}$$

where $F^{-1}[.]$ denotes the inverse Fourier transform, and $C(t)$ is an undetermined function. This indeterminacy in the inverse transform of $1/|\hat{\omega}|$ is discussed by Lighthill (1958) and proves to be crucial in the following analysis. Using (2.66) along with the convolution theorem we can also show that

$$F\left[-\frac{1}{\pi}\log|\hat{x}| + \frac{1}{2\pi}\int_{-\infty}^{\infty}\log|X-\hat{x}|\mathrm{e}^{-|X|}\mathrm{d}X\right] = \frac{|\hat{\omega}|}{1+\hat{\omega}^2}. \tag{2.67}$$

By subtracting this function from the integrand in (2.65) we arrive at

$$Y(\hat{x},t) \sim t^{1/2}|\hat{x}| + tY_1(\hat{x}) \quad \text{as } t \to 0 \text{ for } \hat{x} = O(1), \tag{2.68}$$

where

$$Y_1(\hat{x}) = -\frac{\mathrm{i}}{\pi^2}\int_{c-\mathrm{i}\infty}^{c+\mathrm{i}\infty}\frac{\mathrm{e}^{\sigma}}{\sigma}\int_0^{\infty}\cos\hat{\omega}\hat{x}\left\{\frac{\hat{\omega}}{\left(\sigma+2\hat{\omega}^2\right)^2 - 4\hat{\omega}^3\left(\sigma+\hat{\omega}^2\right)^{1/2}} - \frac{\hat{\omega}}{2\sigma\left(1+\hat{\omega}^2\right)}\right\}\mathrm{d}\hat{\omega}\,\mathrm{d}\sigma$$
$$-\frac{1}{\pi}\log|\hat{x}| + \frac{1}{2\pi}\int_{-\infty}^{\infty}\log|X-\hat{x}|\mathrm{e}^{-|X|}\,\mathrm{d}X. \tag{2.69}$$

There are simpler ways of writing this inverse Fourier transform in terms of ordinary functions, but the formulation given by (2.69) is convenient for numerical evaluation. The function $Y_1(\hat{x})$ is plotted in figure 5. The integrals in (2.69) were evaluated using Simpson's rule, taking care to evaluate the final integral analytically in the neighbourhood of its integrable logarithmic singularity.

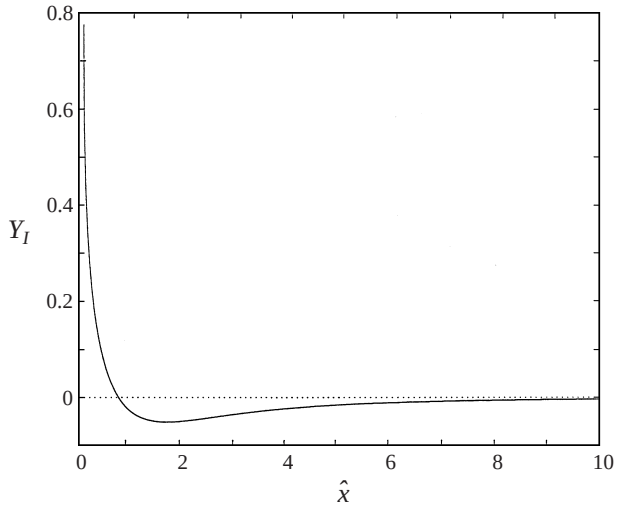

FIGURE 5. The function $Y_1(\hat{x})$.

In order to compare this asymptotic result with the full solution we use

$$Y(x,t) = |x| - \frac{\mathrm{i}}{\pi^2}\int_0^\infty \cos\omega x \int_{c-\mathrm{i}\infty}^{c+\mathrm{i}\infty} \frac{\omega \mathrm{e}^{st}}{s\{\left(s+2\omega^2\right)^2 + \omega^3 - 4\omega^3\left(s+\omega^2\right)^{1/2}\}}\mathrm{d}s\,\mathrm{d}\omega, \tag{2.70}$$

and evaluate the double integral numerically using Simpson's rule. Suitably scaled versions of the asymptotic expression (2.68) for the position of the interface are compared with the numerically evaluated solution in figure 6, and are in excellent agreement.

The expansion (2.68) matches with (2.64) as $\hat{x} \to \infty$, and

$$Y(\hat{x},t) \sim t^{1/2}|\hat{x}| - t\frac{1}{\pi}\log|\hat{x}| + \alpha t \quad \text{as } \hat{x} \to 0, \tag{2.71}$$

where

$$\alpha = -\frac{\mathrm{i}}{\pi^2}\int_{c-\mathrm{i}\infty}^{c+\mathrm{i}\infty}\frac{\mathrm{e}^\sigma}{\sigma} \times \int_0^\infty \left\{\frac{\hat{\omega}}{\left(\sigma+2\hat{\omega}^2\right)^2 - 4\hat{\omega}^3\left(\sigma+\hat{\omega}^2\right)^{1/2}} - \frac{\hat{\omega}}{2\sigma\left(1+\hat{\omega}^2\right)}\right\}\mathrm{d}\hat{\omega}\,\mathrm{d}\sigma - \gamma \approx -0.18, \tag{2.72}$$

and γ is Euler's constant. This becomes non-uniform when $\hat{x} = O(t^{1/2}\log(1/t))$, $x = O(t\log(1/t))$. However, if we return to (2.62) and look for distinguished limits where terms in the integrand balance, we find that a scaling with $x = O(t)$ suggests itself for the next, inner, asymptotic region. This suggests that the non-uniformity where $x = O(t\log(1/t))$ is passive. The divergence between the logarithmic singularity in the asymptotic solution, and the bounded, numerical solution can be seen in figure 6.

We proceed by defining new variables $x = t\bar{x}$ and $\omega = t^{-1}\bar{\omega}$, in terms of which we

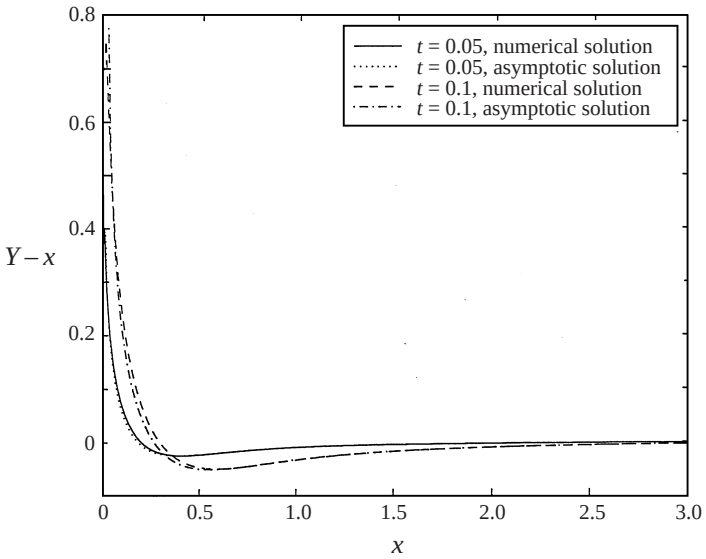

FIGURE 6. The deformation of the interface evaluated both numerically and asymptotically using (2.68) for $t = 0.05$ and 0.1.

find that

$$Y(\bar{x},t) \sim -\frac{2t}{\pi}\int_{-\infty}^{\infty}\frac{\mathrm{e}^{\mathrm{i}\bar{\omega}\bar{x}}}{\bar{\omega}^2}\frac{1}{2\pi\mathrm{i}}\int_{c-\mathrm{i}\infty}^{c+\mathrm{i}\infty}\frac{\sigma^2\mathrm{e}^{\sigma}}{2\sigma+|\bar{\omega}|}\mathrm{d}\sigma\,\mathrm{d}\bar{\omega} \quad \text{as } t\to 0 \text{ for } \bar{x}=O(1). \tag{2.73}$$

The integrand has a simple pole at $\sigma = -\frac{1}{2}|\omega|$, and hence

$$Y(\bar{x},t) \sim -\frac{t}{\pi}\int_{-\infty}^{\infty}\frac{\mathrm{e}^{\mathrm{i}\bar{\omega}\bar{x}-|\bar{\omega}|/2}}{\bar{\omega}^2}\mathrm{d}\bar{\omega} \quad \text{as } t\to 0 \text{ for } \bar{x}=O(1). \tag{2.74}$$

Again, this only exists as a generalized function, since there is a non-integrable singularity at $\bar{\omega}=0$. We therefore write

$$t^{-1}Y(\bar{x},t) \sim -\frac{2}{\pi}\int_0^{\infty}\frac{\cos\bar{\omega}\bar{x}}{\bar{\omega}^2}(\mathrm{e}^{-|\bar{\omega}|/2}-1+\tfrac{1}{2}\bar{\omega})\mathrm{d}\bar{\omega} + |x| - \frac{1}{\pi}\log|\bar{x}| + C(t) \quad \text{as } t\to 0 \text{ for } \bar{x}=O(1). \tag{2.75}$$

The integral is now defined in the usual sense, at least for $\bar{x}>0$, and can be evaluated analytically using the convolution theorem. All that remains is to determine the function $C(t)$. This can be found from matching with expansion (2.71) as $\bar{x}\to\infty$, which shows that

$$C(t) \sim \frac{1}{2\pi}\log(1/t)+\alpha \quad \text{as } t\to 0, \tag{2.76}$$

and hence that

$$Y(\bar{x},t) \sim \frac{t}{\pi}\left\{2\bar{x}\tan^{-1}2\bar{x} - \tfrac{1}{2}\log\left(1+4\bar{x}^2\right) + 1 + \log 2 + \pi\alpha + \tfrac{1}{2}\log(1/t)\right\} \quad \text{as } t\to 0 \text{ for } \bar{x}=O(1). \tag{2.77}$$

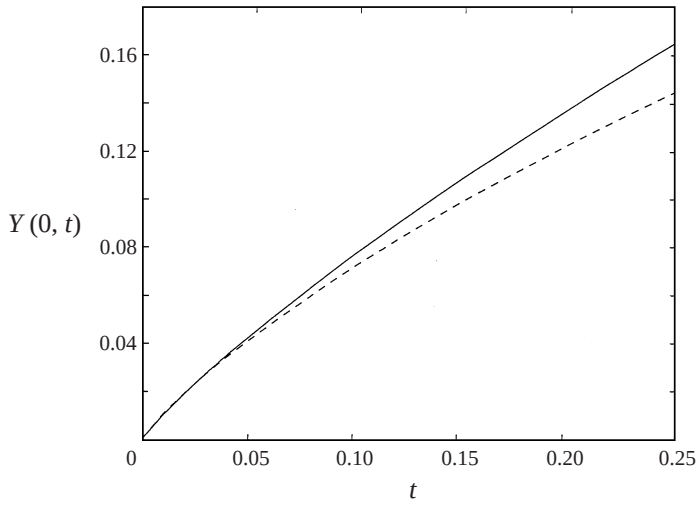

FIGURE 7. A comparison of the position of the tip of the wedge evaluated numerically from (2.70) (solid line), and asymptotically for $t \ll 1$ using (2.78) (broken line).

In particular the tip of the wedge lies at

$$Y(0,t) \sim \frac{t}{\pi}\left(1 + \log 2 + \pi\alpha + \tfrac{1}{2}\log(1/t)\right) \quad \text{as } t \to 0. \tag{2.78}$$

In the inviscid solution, the velocity of the tip was algebraically singular of $O(t^{-1/3})$. We can now see that the effect of viscosity is to weaken this to a logarithmic singularity of $O(\log(1/t))$, but that it does not remove it completely. At first sight, this suggests that there is a problem, since our original assumption was that $\hat{\boldsymbol{u}} = O(\epsilon)$, and now we have found that $\boldsymbol{u}$ is singular near the tip of the wedge as $t \to 0$. However, the only way in which we have used the assumption that $\hat{\boldsymbol{u}} = O(\epsilon)$ is in neglecting the nonlinear term, $\hat{\boldsymbol{u}} \cdot \nabla\hat{\boldsymbol{u}}$, in (2.3). This remains uniformly smaller than the pressure gradient and viscous stress terms on the right-hand side of (2.3), which dominate in the final asymptotic region, where $\boldsymbol{r} = O(t)$. Hence our results are correct at leading order.

We can now compare the asymptotic solution in this final region with the full solution by evaluating (2.70) numerically using Simpson's rule. The asymptotic expression (2.78) for the position of the tip of the wedge is compared with the numerically evaluated solution in figure 7, and is in excellent agreement. We can also use (2.68) and (2.77) to construct a composite solution

$$\begin{aligned} Y(x,t) \sim\ & -\frac{\mathrm{i}t}{\pi^2}\int_{c-\mathrm{i}\infty}^{c+\mathrm{i}\infty}\frac{\mathrm{e}^{\sigma}}{\sigma} \\ & \times\int_0^{\infty}\cos\hat{\omega}\hat{x}\left\{\frac{\omega}{\left(\sigma+2\hat{\omega}^2\right)^2-4\hat{\omega}^3\left(\sigma+\hat{\omega}^2\right)^{1/2}}-\frac{\hat{\omega}}{2\sigma\left(1+\hat{\omega}^2\right)}\right\}\mathrm{d}\hat{\omega}\,\mathrm{d}\sigma \\ & +\frac{t}{2\pi}\int_{-\infty}^{\infty}\log|X-\hat{x}|\mathrm{e}^{-|X|}\mathrm{d}X+\frac{t}{\pi}\left\{2\bar{x}\tan^{-1}2\bar{x}-\tfrac{1}{2}\log\left(1+4\bar{x}^2\right)\right. \\ & \left.+1+\log 2+\tfrac{1}{2}\log(1/t)\right\} \quad \text{as } t\to 0 \text{ for } x \geqslant 0. \end{aligned} \tag{2.79}$$

This composite solution is compared with the solution evaluated numerically using

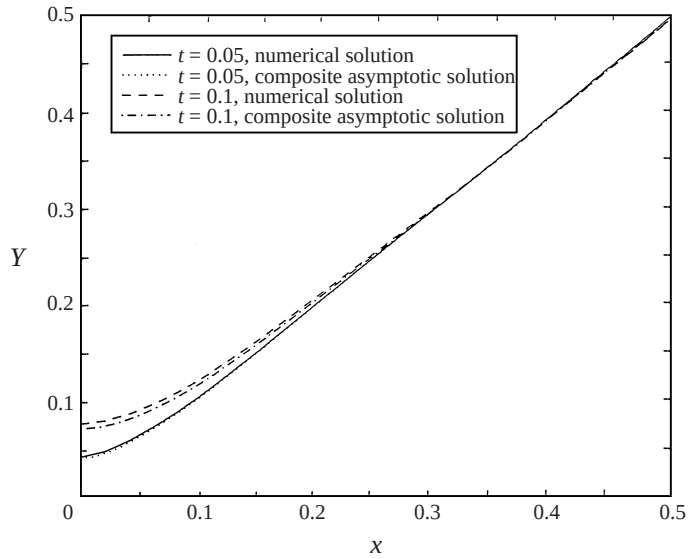

FIGURE 8. The deformation of the interface evaluated both numerically from (2.70) and asymptotically using the composite solution (2.79) for $t = 0.05$ and 0.1.

(2.70) at $t = 0.05$ and 0.1 in figure 8. We expect the difference between the numerical and asymptotic solutions to be of $O(t^2)$, consistent with figure 8.

Having determined the order of magnitude of the deformation of the free surface, we can use the same approach to find the size of the fluid pressure and velocity using (2.62). When $x = O(t^{1/2})$ and $y = O(t^{1/2})$, $p = O(t^{-1/2})$, $\boldsymbol{u} = O(1)$ and $Y = O(t)$. This means that all three terms in the momentum equation, (2.12), appear at leading order, but that the term Y_{xx}, which models the effect of surface tension, is absent at leading order from the Bernoulli condition, (2.16). When $x = O(t)$ and $y = O(t)$, $p = O(t^{-1})$, $u_x = O(1)$, $u_y = -(\log t)/2\pi + O(1)$ and $Y = -t(\log t)/2\pi + O(t)$. In this case, the inertial term, $\partial \boldsymbol{u}/\partial t$, does not appear at leading order in (2.12), and the bulk flow is dominated by viscosity. However, all three terms in (2.16) appear at leading order. Note that the spatially uniform translation of the $O(t)$ tip region at a speed of $O(\log t)$ is analagous to the behaviour during viscous pinchoff of a thread, investigated by Lister & Stone (1998). They deduced this scaling by considering the Stokes flow induced by surface tension in a fixed cone of viscous fluid. To summarize, when $x, y = O(t^{1/2})$ the flow is dominated by inertia and viscosity, whilst for $x, y = O(t)$ the flow is dominated by viscosity and surface tension.

2.4.2. *The deformation of the interface for $t \gg 1$*

For $t \gg 1$ we expect the inviscid solution, which we examined in § 2.2, to emerge at leading order. If we define $\xi = x/t^{2/3}$, $\tilde{\omega} = \omega t^{2/3}$ and substitute into (2.62) we find that

$$Y(\xi, t) \sim \frac{t^{2/3}}{2\pi} \int_{-\infty}^{\infty} \mathrm{e}^{\mathrm{i}\tilde{\omega}\xi} \frac{1}{2\pi\mathrm{i}} \int_{c-\mathrm{i}\infty}^{c+\mathrm{i}\infty} \frac{2|\tilde{\omega}|\mathrm{e}^{\sigma}}{\sigma} \left\{ \frac{1}{\left(\sigma + 2t^{-1/3}\tilde{\omega}^2\right)^2 + |\tilde{\omega}|^3} - \frac{1}{|\tilde{\omega}|^3} \right\} \mathrm{d}\sigma \, \mathrm{d}\tilde{\omega}$$

$$\text{as } t \to \infty \text{ for } \xi = O(1). \quad (2.80)$$

If we neglect the term of $O(t^{-1/3})$ we obtain precisely the inviscid solution, which reduces to (2.38). In order to examine the correction due to viscosity it is convenient

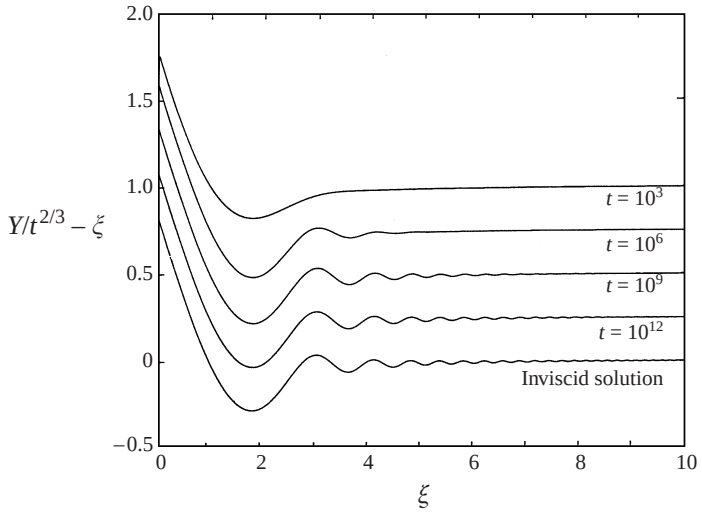

FIGURE 9. The deformation of the interface calculated from the asymptotic solution valid for $t \gg 1$, (2.81), when $t = 10^3$, 10^6, 10^9 and 10^{12} compared with the inviscid solution, (2.38). The asymptotic solutions have been displaced by multiples of 0.25 so that the differences are visible.

to consider the asymptotic solution in the form (2.80). The integrand has poles at $\sigma = \pm \mathrm{i}|\tilde{\omega}|^{3/2} - 2t^{-1/3}\tilde{\omega}^2$, and a straightforward residue calculation shows that

$$Y(\xi, t) = t^{2/3}\left[|\xi| - \frac{2}{\pi}\int_0^\infty \frac{\cos\tilde{\omega}\xi}{\tilde{\omega}^2}\left\{1 - \cos\tilde{\omega}^{3/2}\exp\left(-2t^{-1/3}\tilde{\omega}^2\right)\right\}\mathrm{d}\tilde{\omega}\right] + O(t^{1/3})$$

$$\text{as } t \to \infty \text{ for } \xi = O(1). \quad (2.81)$$

We can evaluate this integral numerically for various values of t using the NAG routine D01ASF, an algorithm for evaluating oscillatory integrals. Some solutions are shown in figure 9, along with the inviscid solution, $Y_I(\xi)$. When $t = 10^3$ the solution looks qualitatively similar to the solution for $t \ll 1$, with a single minimum. When $t = 10^6$ capillary waves are beginning to emerge. The remaining two solutions, for $t = 10^9$ and 10^{12}, show how the extent of the waves on the surface, in terms of the similarity variable, $\xi = x/t^{2/3}$, increases as t increases. When $t = 10^{12}$ the asymptotic solution is indistinguishable from the inviscid solution for $0 \leqslant \xi \leqslant 10$. Note that we have not attempted to compare this asymptotic solution with the numerical solution of the full problem, since it is extremely difficult to evaluate the double integral (2.70) for such large values of t.

We can quantify these observations by considering more carefully the behaviour of the integral in (2.81), which is the same as that in (2.37), but with an extra exponential in the integrand. If we analyse (2.81) for $|\xi| \gg 1$ by evaluating the contribution from the neighbourhood of $\tilde{\omega} = 0$ and the point of stationary phase at $\tilde{\omega} = \frac{4}{9}\xi^2$, we find that

$$Y(\xi, t) \sim t^{2/3}\left\{|\xi| - \frac{1}{\pi\xi^2} - \frac{27}{4\pi^{1/2}|\xi|^{7/2}}\sin\left(\frac{4|\xi|^3}{27} + \frac{\pi}{4}\right)\exp\left(-\frac{32}{81}\xi^4 t^{-1/3}\right)\right\}$$

$$\text{for } |\xi| \gg 1. \quad (2.82)$$

The extra exponential in the integrand leads to damping of the capillary waves in the far field. More precisely, the inviscid solution provides the leading-order solution

for $\xi \ll t^{1/12}$, $x \ll t^{3/4}$. We should now rescale into an asymptotic region where $\xi = O(t^{1/12})$, $x = O(t^{3/4})$, but we find that this region is passive and simply reproduces the far-field solution, (2.82), at leading order. For $\xi \gg t^{1/12}$, $x \gg t^{3/4}$, the capillary waves are exponentially damped by viscosity. This is consistent with the results presented in figure 9.

One possible difficulty with these solutions is that, since $Y \sim x$ as $x \to \infty$, our assumption that $\hat{Y} = \epsilon Y = O(\epsilon)$ is not valid when $x = O(\epsilon^{-1})$. First, we note that the terms involving Y that we have neglected in the governing equations are all x-derivatives of Y, and hence remain uniformly small as $x \to \infty$. The only possible problem lies in applying the boundary conditions at $y = 0$, rather than $y = \epsilon Y$. However, in the far field we expect that all of the dependent variables are functions of $\sqrt{x^2 + y^2}$, and hence, on the boundary, functions of $\sqrt{x^2 + \epsilon^2 Y^2}$. This means that even when $x = O(\epsilon^{-1})$ our approximation remains valid.

3. The fat cone

3.1. *Formulation of the initial/boundary value problem*

Consider an initially stationary cone of incompressible fluid with semi-angle $\pi/2 - \tan^{-1}\epsilon$. In this case we work in cylindrical polar coordinates, (r, θ, z), and seek an axisymmetric solution. The position of the free surface is given by $z = Z(r, t)$, as illustrated in figure 1 substituting r for x, z for y and Z for Y. Proceeding as in § 2, we non-dimensionalize using scales (2.1) and linearize to obtain the leading-order problem for $|\epsilon| \ll 1$,

$$\psi_{zt} = -p_r + \psi_{rrz} + \psi_{zzz} + \frac{1}{r}\psi_{rz} - \frac{1}{r^2}\psi_z \quad \text{for } z \geqslant 0, \tag{3.1}$$

$$p_{rr} + \frac{1}{r}p_r + p_{zz} = 0 \quad \text{for } z \geqslant 0, \tag{3.2}$$

$$Z_t = -\psi_r - \frac{1}{r}\psi \quad \text{at } z = 0, \tag{3.3}$$

$$\psi_{rr} + \frac{1}{r}\psi_r + \frac{1}{r^2}\psi = \psi_{zz} \quad \text{at } z = 0, \tag{3.4}$$

$$p + 2\psi_{rz} + \frac{2}{r}\psi_z = Z_{rr} + \frac{1}{r}Z_r \quad \text{at } z = 0, \tag{3.5}$$

$$\psi = 0, \quad Z = r \quad \text{when } t = 0, \tag{3.6}$$

$$\psi \to 0, \quad p \to 0 \quad \text{as } r^2 + z^2 \to \infty, \tag{3.7}$$

$$Z = r + o(1) \quad \text{as } r \to \infty, \tag{3.8}$$

which is the initial/boundary value problem for the fat cone equivalent to (2.20) to (2.27) for the fat wedge, with the radial and axial components of the velocity given by $u_r = \psi_z$ and $u_z = -\psi_r$. Note that, physically, the main difference is that there is curvature about the z-axis, which manifests itself as the extra term $(1/r)Z_r$ in (3.5). This term is equal to $1/r$ when the cone is undisturbed, with $Z = r$, so that surface tension immediately induces a flow at infinity.

3.2. *The linearized inviscid problem*

For a fat inviscid cone, (3.1) and (3.5) become

$$\psi_{zt} = -p_r \quad \text{for } z \geqslant 0, \quad \text{and} \quad p = Z_{rr} + \frac{1}{r}Z_r \quad \text{at } z = 0, \tag{3.9}$$

whilst (3.4) cannot be satisfied. We proceed by defining Hankel–Laplace transforms as

$$\tilde{Z}(v,s) = \int_0^\infty \mathrm{e}^{-st} \int_0^\infty rJ_0(vr)Z(r,t)\mathrm{d}r\,\mathrm{d}t, \tag{3.10}$$

$$\tilde{p}(v,z,s) = \int_0^\infty \mathrm{e}^{-st} \int_0^\infty rJ_0(vr)p(r,z,t)\mathrm{d}r\,\mathrm{d}t, \tag{3.11}$$

$$\tilde{\psi}(v,z,s) = \int_0^\infty \mathrm{e}^{-st} \int_0^\infty rJ_1(vr)p(r,z,t)\mathrm{d}r\,\mathrm{d}t. \tag{3.12}$$

The inviscid problem is thereby reduced to

$$s\tilde{\psi}_z = v\tilde{p} \quad \text{for } z \geqslant 0, \tag{3.13}$$

$$\tilde{p}_{zz} - v^2\tilde{p} = 0 \quad \text{for } z \geqslant 0, \tag{3.14}$$

$$s\tilde{Z} + \frac{1}{v^3} = -v\tilde{\psi} \quad \text{at } z = 0, \tag{3.15}$$

$$\tilde{p} = -v^2\tilde{Z} \quad \text{at } z = 0, \tag{3.16}$$

$$\tilde{\psi} \to 0, \quad \tilde{p} \to 0 \quad \text{as } z \to \infty. \tag{3.17}$$

Note that we have made use of the fact that, as a generalized function, the order-zero Hankel transform of r is $-1/v^3$. Further details concerning Hankel transforms of generalized functions are given in the Appendix (see also Misra & Lavoine 1986).

It is easy to show that

$$\tilde{p} = \frac{s\mathrm{e}^{-vz}}{v(s^2+v^3)}, \quad \tilde{\psi} = -\frac{\mathrm{e}^{-vz}}{v(s^2+v^3)}, \quad \tilde{Z} = -\frac{s}{v^3(s^2+v^3)}. \tag{3.18}$$

Proceeding as for the fat wedge, we let $\xi = r/t^{2/3}$, and perform a residue calculation to find that

$$Z(\xi,t) = t^{2/3}Z_I(\xi) = t^{2/3}\left\{\xi + \int_0^\infty J_0(v\xi)\frac{1-\cos v^{3/2}}{v^2}\mathrm{d}v\right\}. \tag{3.19}$$

The function Z_I can be calculated numerically using Simpson's rule, and is illustrated in figure 10. As for the fat wedge, the tip of the fat cone is blunted by the action of surface tension, and capillary waves propagate away on the free surface. Note that

$$Z_I(0) = \tfrac{1}{2}\pi Y_I(0). \tag{3.20}$$

In other words, the tip of a fat inviscid cone snaps back a distance $\pi/2 \approx 1.57$ times further than the tip of a fat wedge, as the extra curvature about the z-axis causes surface tension to pull it back more strongly. Note also that, since $\tilde{\psi} \sim -\mathrm{e}^{-vz}/vs^2$ as $v \to 0$,

$$\psi \sim \frac{t}{r}\left(1 - \frac{z}{\sqrt{r^2+z^2}}\right) \quad \text{for } r^2 + z^2 \gg 1, \tag{3.21}$$

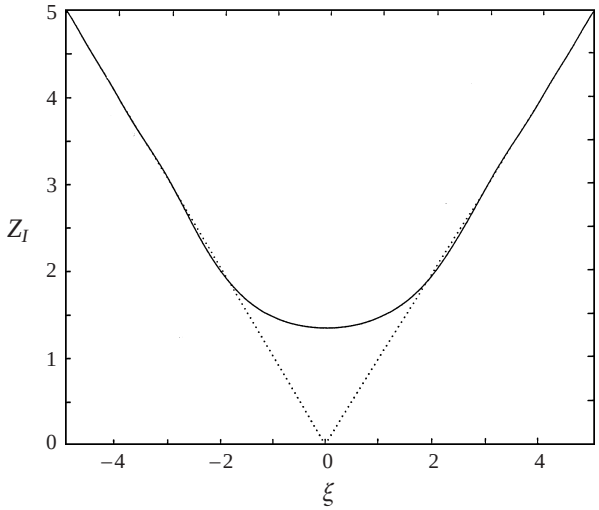

FIGURE 10. The function $Z_I(\xi)$ (solid line) and the initial position of the interface (dotted line).

and hence

$$u_z \sim \frac{tz}{\left(r^2+z^2\right)^{3/2}} \quad \text{for } r^2+z^2 \gg 1, \tag{3.22}$$

and

$$2\pi \int_0^\infty r u_z \mathrm{d}r \sim 2\pi t \quad \text{for } z \gg 1. \tag{3.23}$$

This means that in the far field there is a non-zero total flux of fluid through any plane where z is constant, which increases linearly with t. This occurs because the curvature of the free surface is non-zero in the far field and drives an acceleration of the fluid. This is not the case for the fat wedge, where there is no curvature in the far field, and hence no net flux of fluid. This means that the area under the curve $y = Y_I - |x|$ must be zero, by conservation of mass, but that this is not true for the curve $z = Z_I - r$.

We can determine the behaviour of Z_I in the far field, proceeding as for the fat wedge (see the Appendix), and find that

$$Z_I \sim \xi - \left\{\frac{2}{3} + \frac{81}{8\sqrt{2}} \sin\left(\frac{4}{27}\xi^3\right)\right\} \frac{1}{\xi^5} \quad \text{for } \xi \gg 1. \tag{3.24}$$

For the fat wedge, (2.42), the deformation of the interface is of $O(1/\xi^2)$ as $\xi \to \infty$, whilst the amplitude of the capillary waves is of $O(1/\xi^{7/2})$. The behaviour for the fat cone is dramatically different, with both the deformation of the interface and the amplitude of the capillary waves much smaller, of $O(1/\xi^5)$. This is due to a combination of the geometrical effect of the spreading of the waves and the extra surface tension force caused by the curvature about the z-axis. This is illustrated in figure 11, where the envelope of the capillary waves, given by

$$Z_e(\xi) = -\left(\frac{2}{3} \pm \frac{81}{8\sqrt{2}}\right) \frac{1}{\xi^5}, \tag{3.25}$$

is plotted against $Z_I - \xi$, evaluated numerically using Simpson's rule, and is in excellent

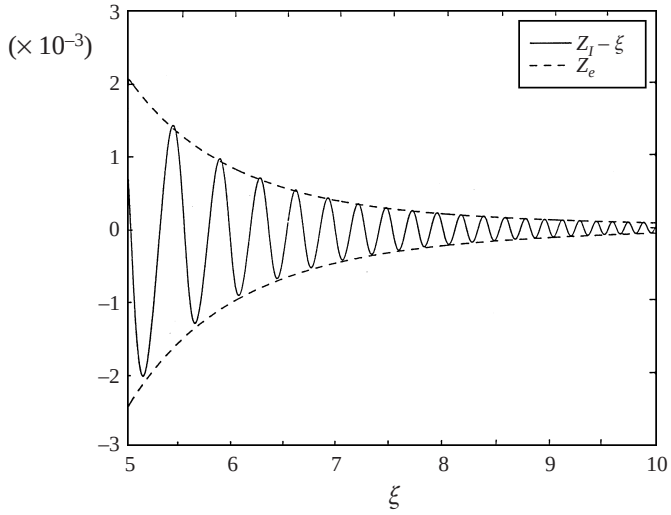

FIGURE 11. The deformation of the interface, $Z_I(\xi) - \xi$, (solid line) and the far-field envelope of the capillary waves, $Z_e(\xi)$, (broken line).

agreement. Note that we have not attempted to resolve the high-frequency oscillations given by (3.24) in this numerical solution. In addition, we note that the wavelength of the capillary waves is $27\pi/2\xi^2$, the same as for the fat wedge, but that there is a phase difference of $\pi/4$ between the waves in the far field of the fat wedge and those of the fat cone.

3.3. *The full linearized problem*

The Hankel–Laplace transform of the solution of the full linearized problem, (3.1) to (3.8), is

$$\left.\begin{aligned} \tilde{p} &= \frac{(s+2v^2)\mathrm{e}^{-vz}}{vK(v,s)}, \\ \tilde{\psi} = -\frac{v}{sK(v,s)}\left\{\frac{(s+2v^2)\mathrm{e}^{-vz}}{v^2} - 2\mathrm{e}^{-(s+v^2)^{1/2}z}\right\}, &\quad \tilde{Z} = \frac{1}{s}\left(\frac{1}{K(v,s)} - \frac{1}{v^3}\right), \end{aligned}\right\} \tag{3.26}$$

where

$$K(v,s) = (s+2v^2)^2 + v^3\{1 - 4\left(s+v^2\right)^{1/2}\}. \tag{3.27}$$

3.3.1. *The deformation of the interface for $t \ll 1$*

We proceed exactly as we did for the fat wedge, and conclude that the same asymptotic structure emerges. We find that

$$Z(r,t) \sim r + \frac{192}{35\sqrt{\pi}}\frac{t^{7/2}}{r^5} \quad \text{for } r \gg t^{1/2}. \tag{3.28}$$

There are corrections to this asymptotic expansion that are exponentially small provided $r \gg t^{1/2}$. Further details of this calculation are given in the Appendix. In order to compare this asymptotic result with the full solution we use

$$Z(r,t) = r - \frac{\mathrm{i}}{2\pi}\int_0^\infty J_0(vr)\int_{c-\mathrm{i}\infty}^{c+\mathrm{i}\infty}\frac{v\mathrm{e}^{st}}{s\{\left(s+2v^2\right)^2 + v^3 - 4v^3\left(s+v^2\right)^{1/2}\}}\mathrm{d}s\,\mathrm{d}v, \tag{3.29}$$

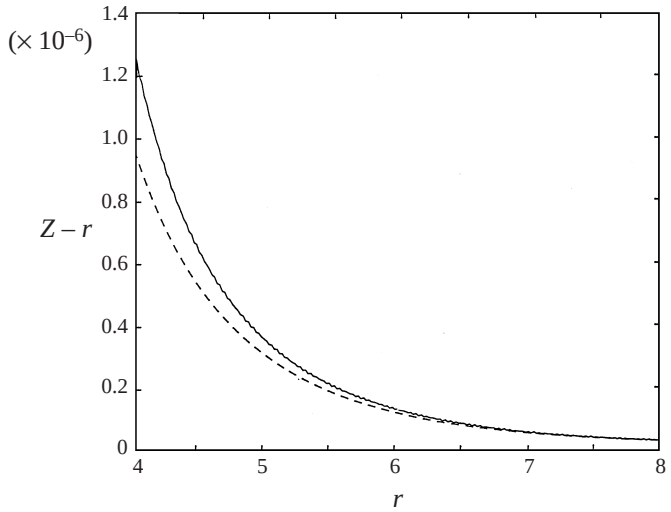

FIGURE 12. Comparison of the deformation of the interface when $t = 0.1$ calculated numerically from (3.29) (solid line) and asymptotically, (3.28) (broken line).

and evaluate the double integral numerically using Simpson's rule. Figure 12 shows a comparison between the position of the interface when $t = 0.1$ calculated numerically from (3.29) and the asymptotic behaviour given by (3.28). The agreement between the two is excellent. Note that the numerical solution is rather ragged due to the difficulty in calculating such small deformations accurately without being wasteful of c.p.u. time.

We can examine the deformation of the interface when $r = O(t^{1/2})$ by defining $r = t^{1/2}\hat{r}$, $v = t^{-1/2}\hat{v}$. We find that

$$Z(\hat{r},t) \sim t^{1/2}\hat{r} + tZ_1(\hat{r}) \quad \text{as } t \to 0 \text{ for } \hat{r} = O(1), \tag{3.30}$$

where

$$Z_1(\hat{r}) = -\frac{\mathrm{i}}{2\pi}\int_{c-\mathrm{i}\infty}^{c+\mathrm{i}\infty}\frac{\mathrm{e}^{\sigma}}{\sigma}\int_0^{\infty} J_0(\hat{v}\hat{r}) \times\left\{\frac{\hat{v}}{\left(\sigma+2\hat{v}^2\right)^2-4\hat{v}^3\left(\sigma+\hat{v}^2\right)^{1/2}}-\frac{\hat{v}}{2\sigma\left(\hat{v}^4+4\right)^{1/2}}\right\}\mathrm{d}\hat{v}\,\mathrm{d}\sigma+\tfrac{1}{2}J_0(\hat{r})K_0(\hat{r}). \tag{3.31}$$

The function $Z_1(\hat{r})$ is plotted in figure 13. The integrals in (3.31) were evaluated using Simpson's rule. Suitably scaled versions of the asymptotic expression (3.30) for the position of the interface are compared with the numerically evaluated solution in figure 14, and are in excellent agreement for $r \gg t$.

We find that

$$Z(\hat{r},t) \sim t^{1/2}\hat{r} - t\tfrac{1}{2}\log\hat{r} + \beta t \quad \text{as } \hat{r} \to 0, \tag{3.32}$$

where

$$\beta = -\frac{\mathrm{i}}{2\pi}\int_{c-\mathrm{i}\infty}^{c+\mathrm{i}\infty}\frac{\mathrm{e}^{\sigma}}{\sigma}\int_0^{\infty}\left\{\frac{\hat{v}}{\left(\sigma+2\hat{v}^2\right)^2-4\hat{v}^3\left(\sigma+\hat{v}^2\right)^{1/2}}-\frac{\hat{v}}{2\sigma\left(4+\hat{v}^4\right)^{1/2}}\right\}\mathrm{d}\hat{v}\,\mathrm{d}\sigma + \tfrac{1}{2}(\log 2-\gamma) \approx 0.065. \tag{3.33}$$

The divergence between the logarithmic singularity in the asymptotic solution, and the

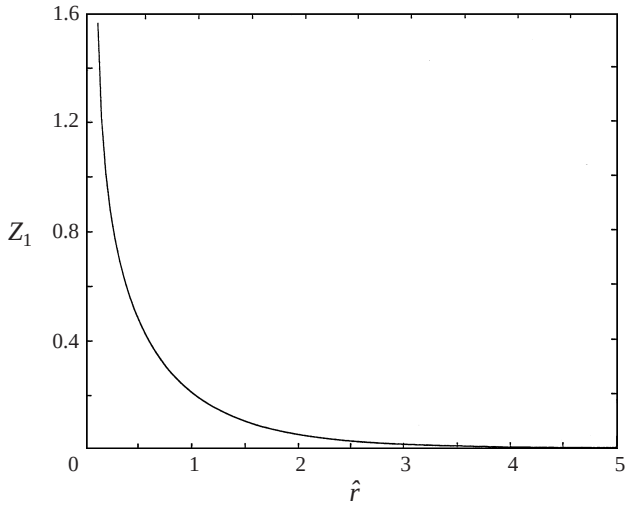

FIGURE 13. The function $Z_1(\hat{r})$.

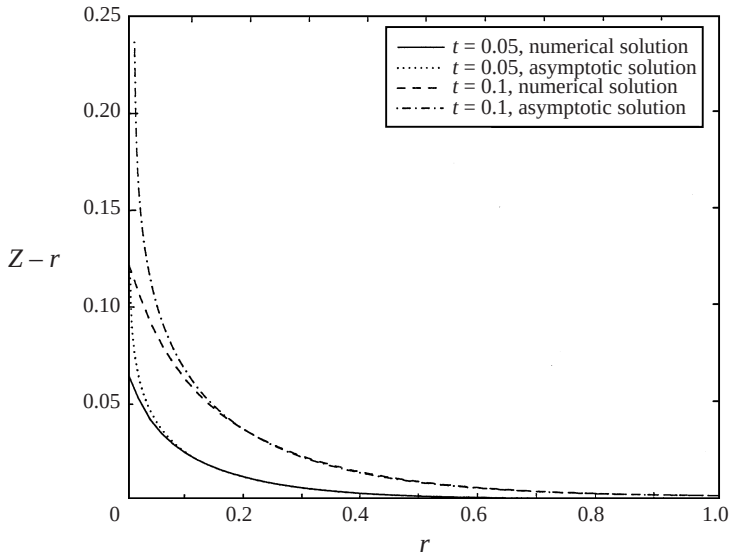

FIGURE 14. The deformation of the interface evaluated both numerically and asymptotically for $t = 0.05$ and 0.1.

bounded, numerical solution can be seen in figure 14, and is rather more pronounced than for the wedge, figure 6, due to the different scales of the horizontal axes.

In order to construct the solution in the final asymptotic region, we define new variables $r = t\bar{r}$ and $v = t^{-1}\bar{v}$ and, after a simple residue calculation, find that

$$Z(\bar{r}, t) \sim -t \int_0^\infty J_0(\bar{v}\bar{r}) \frac{\mathrm{e}^{-\bar{v}/2}}{\bar{v}^2} \mathrm{d}\bar{v} \quad \text{as } t \to 0 \text{ for } \bar{r} = O(1). \tag{3.34}$$

Again, this only exists as a generalized function, since there is a non-integrable

singularity at $\bar{v} = 0$. We therefore write

$$t^{-1}Z(\bar{r},t) \sim -\int_0^\infty \frac{J_0(\bar{v}\bar{r})}{\bar{v}^2}(\mathrm{e}^{-\bar{v}/2} - 1 + \tfrac{1}{2}\bar{v})\mathrm{d}\bar{v} + \bar{r} - \tfrac{1}{2}\log\bar{r} + D(t)$$
$$\text{as } t \to 0 \text{ for } \bar{r} = O(1). \quad (3.35)$$

We must now determine the asymptotic behaviour of the unknown function of time, $D(t)$, by matching with the previous region. We find that

$$D(t) \sim \tfrac{1}{4}\log(1/t) + \beta \quad \text{for } t \ll 1, \quad (3.36)$$

and hence that the tip of the cone lies at

$$Z(0,t) \sim t\left(\tfrac{1}{4}\log(1/t) + \beta + \delta\right) \quad \text{as } t \to 0, \quad (3.37)$$

where

$$\delta = \lim_{\bar{r}\to 0}\left[\int_0^\infty \frac{J_0(\bar{v}\bar{r})}{\bar{v}^2}(1 - \tfrac{1}{2}\bar{v} - \mathrm{e}^{-\bar{v}/2})\mathrm{d}\bar{v} - \tfrac{1}{2}\log\bar{r}\right] \approx 0.50. \quad (3.38)$$

As for the fat wedge, viscosity weakens the initial singularity in the velocity from $O(t^{-1/3})$ to $O(\log(1/t))$. In addition, as we saw for the inviscid solution, (3.20), the tip of the cone moves $\pi/2$ times faster than that of the wedge, at leading order for $t \ll 1$, since

$$Z(0,t) \sim \tfrac{1}{2}\pi Y(0,t) \quad \text{as } t \to 0. \quad (3.39)$$

We can now compare the asymptotic solution in this final region with the full solution by evaluating (3.29) numerically using Simpson's rule. The asymptotic expression (3.37) for the position of the tip of the wedge is compared with the numerically evaluated solution in figure 15, and is in excellent agreement. We can also construct a composite solution

$$Z(r,t) \sim tZ_1(\hat{r}) - t\int_0^\infty \frac{J_0(\bar{v}\bar{r})}{\bar{v}^2}(\mathrm{e}^{-\bar{v}/2} - 1 + \tfrac{1}{2}\bar{v})\mathrm{d}\bar{v} \quad \text{as } t \to 0 \text{ for } r \geqslant 0. \quad (3.40)$$

This composite solution is compared with the solution evaluated numerically using (3.29) at $t = 0.05$ and 0.1 in figure 16. We expect the difference between the numerical and asymptotic solutions to be of $O(t^2)$, consistent with figure 16.

3.3.2. *The deformation of the interface for $t \gg 1$*

If we define $\xi = r/t^{2/3}$, $\tilde{v} = vt^{2/3}$ and substitute into (3.29) we find that

$$Z(\xi,t) \sim t^{2/3}\int_0^\infty \tilde{v}J_0(\tilde{v}\xi)\frac{1}{2\pi\mathrm{i}}\int_{c-\mathrm{i}\infty}^{c+\mathrm{i}\infty}\frac{\mathrm{e}^\sigma}{\sigma}\left\{\frac{1}{\left(\sigma + 2t^{-1/3}\tilde{v}^2\right)^2 + \tilde{v}^3} - \frac{1}{\tilde{v}^3}\right\}\mathrm{d}\sigma\,\mathrm{d}\tilde{v}$$
$$\text{as } t \to \infty \text{ for } \xi = O(1). \quad (3.41)$$

A residue calculation shows that

$$Z(\xi,t) = t^{2/3}\left[\xi - \int_0^\infty \frac{J_0(\tilde{v}\xi)}{\tilde{v}^2}\left\{1 - \cos\tilde{v}^{3/2}\exp\left(-2t^{-1/3}\tilde{v}^2\right)\right\}\mathrm{d}\tilde{v}\right] + O(t^{1/3})$$
$$\text{as } t \to \infty \text{ for } \xi = O(1). \quad (3.42)$$

We can evaluate this integral numerically for various values of t using Simpson's rule. Some solutions are shown in figure 17, along with the inviscid solution, $Z_I(\xi)$. The behaviour is qualitatively the same as for the fat wedge, although the capillary waves have a much smaller amplitude, as discussed in § 3.2. We can again

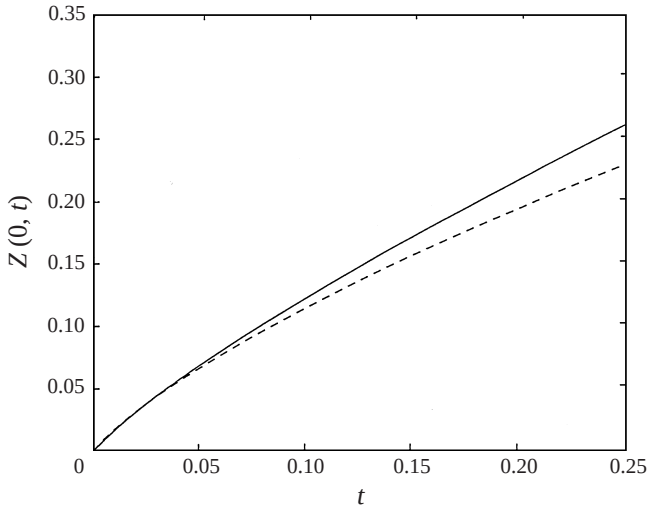

FIGURE 15. A comparison of the position of the tip of the cone evaluated numerically from (3.29) (solid line), and asymptotically for $t \ll 1$ using (3.37) (broken line).

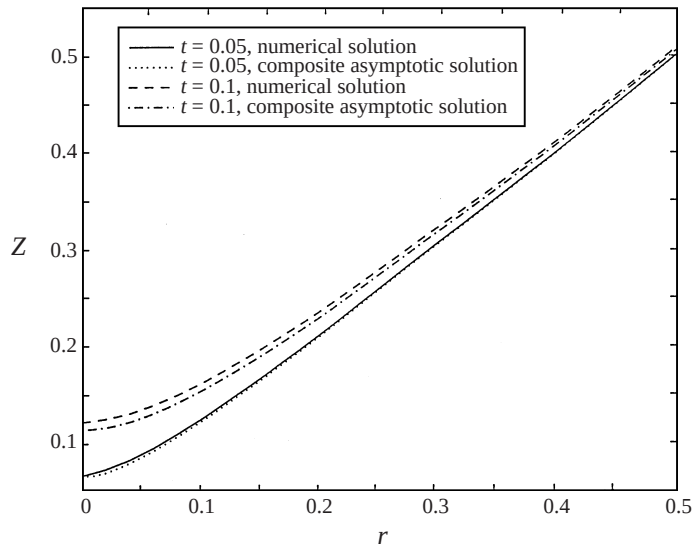

FIGURE 16. The deformation of the interface evaluated both numerically from (3.29) and asymptotically using the composite solution (3.40) for $t = 0.05$ and 0.1.

quantify this observation by considering more carefully the behaviour of the integral in (3.42). If we analyse (3.42) for $\xi \gg 1$ by evaluating the contribution from the neighbourhood of $\tilde{v} = 0$ and the point of stationary phase, we find that

$$Z(\xi, t) \sim \xi - \frac{1}{\xi^5}\left\{\frac{2}{3} + \frac{81}{8\sqrt{2}}\sin\left(\frac{4}{27}\xi^3\right)\exp\left(-\frac{32}{81}\xi^4 t^{-1/3}\right)\right\} \quad \text{for } \xi \gg 1. \qquad (3.43)$$

The extra exponential in the integrand leads to damping of the capillary waves in the far field, consistent with the results presented in figure 17. Note that this means, both for the fat wedge and the fat cone, that significant numbers of capillary waves

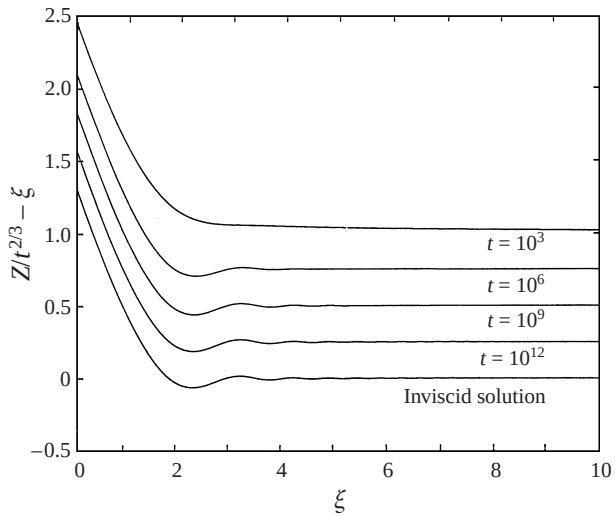

FIGURE 17. The deformation of the interface calculated from the asymptotic solution valid for $t \gg 1$, (3.42), when $t = 10^3$, 10^6, 10^9 and 10^{12} compared with the inviscid solution, (3.19). The asymptotic solutions have been displaced by multiples of 0.25 so that the differences are visible.

are only generated when $t^{1/12}$ is sufficiently large. This, along with the rapid rate of decay of the amplitude of the waves on the fat cone, provides some insight into why few capillary waves are seen on the surface of a droplet immediately after it detaches from a dripping tap (Peregrine *et al.* 1990).

4. Conclusions

In this paper we have analysed the effect of viscosity on the surface-tension-driven deformation of wedges and cones with semi-angles close to $\pi/2$. We have shown the following:

(*a*) The singularity in the fluid velocity as $t \to 0$ is reduced from $O(t^{-1/3})$ for the inviscid solution to $O(\log(1/t))$ for the linearized, viscous solution.

(*b*) For $t \ll 1$ there is an inner, tip region with size of $O(t)$, dominated by surface tension and viscosity, and an outer region with size of $O(t^{1/2})$, dominated by inertia and viscosity.

(*c*) For $t \ll 1$, the tip of the cone moves $\pi/2$ times faster than that of the wedge.

(*d*) For $t \gg 1$, the deformation of the interface asymptotes to the inviscid solution in the region where $x \ll t^{3/4}$ for the wedge, $r \ll t^{3/4}$ for the cone.

(*e*) The capillary waves on the interface are damped out by viscosity for distances of $O(t^{3/4})$ from the tip for $t \gg 1$, and hence $t^{1/12}$ must be large for significant numbers of capillary waves to be observed on the free surface.

We have also been able to compare the behaviour of the inviscid wedge and cone in this limit and found the following:

(*a*) The tip of the cone moves $\pi/2$ times faster than that of the wedge.

(*b*) The rate of decay of the mean deformation of the surface in the far field is of $O(1/x^2)$ for the wedge and $O(1/r^5)$ for the cone.

(*c*) The rate of decay of the amplitude of the capillary waves in the far field is of $O(1/x^{7/2})$ for the wedge and $O(1/r^5)$ for the cone.

(*d*) The wavelengths of the capillary waves in the far field are identical, $27\pi/2x^2$ or $27\pi/2r^2$, for the wedge and the cone.

The methods used in this paper could be extended to account for the presence of an outer fluid, with results relevant to the situation studied by Lister & Stone (1998). It is also of interest to know whether the asymptotic structure of the small- and large-time solutions is also appropriate for wedges and cones that are not fat ($\epsilon = O(1)$).

I would like to thank Professor Andy King for his helpful comments on the final draft of this paper.

Appendix. Hankel transforms of generalized functions

In comparison to the straightforward explanation of the use of Fourier transforms of generalized functions given by Lighthill (1958), the literature on Hankel transforms of generalized functions is rather more obscure as far as an applied mathematician is concerned. The most useful account is probably that given by Misra & Lavoine (1986). In particular, we are interested in the zero-order Hankel transform, $H_0[r^n]$, of powers of r, which is given as an example by Misra & Lavoine, p. 280. Their definition of the Hankel transform is slightly different to that used here, and we find that

$$H_0[r^n] = \frac{2^{n+1}}{\nu^{n+2}} \frac{\Gamma\left(1 + \frac{1}{2}n\right)}{\Gamma\left(-\frac{1}{2}n\right)} \tag{A 1}$$

for n not equal to an even integer. Taken at face value, (A 1) indicates that when n is a positive even integer or zero, the Hankel transform of r^n is zero. We shall see below that when we are estimating inverse Hankel transforms asymptotically, this is indicative of exponentially small, rather than algebraic, behaviour, and hence that we can usually use (A 1) unless n is a negative even integer. These awkward negative even values of n are associated with combinations of powers and logarithms. In particular, by using the identity

$$H_0[f(x)] = -\frac{1}{\nu} H_1[f'(x)], \tag{A 2}$$

where a prime denotes differentiation and $H_1[.]$ is the Hankel transform of order one, we can see that

$$H_0[\log x] = -\frac{1}{\nu^2}. \tag{A 3}$$

Since the Hankel transform has the property of being its own inverse, this formula gives

$$H_0\left[\frac{1}{x^2}\right] = -\log \nu + C, \tag{A 4}$$

where C is an undetermined constant that arises for the reasons outlined by Lighthill (1958) for Fourier transforms. Further applications of similar identities gives, for example,

$$H_0[x^2 \log x] = \frac{4}{\nu^4}, \tag{A 5}$$

although this is not needed in the analysis presented here.

Analysis of the far field of the inviscid linearized solution for the cone

Equation (3.19) shows that

$$Z_I(\xi) = -H_0\left[\frac{\cos v^{3/2}}{v^3}\right]. \tag{A 6}$$

In order to approximate this for $\xi \gg 1$ we must consider the asymptotic behaviour for $v \ll 1$. Since

$$\frac{\cos v^{3/2}}{v^3} \sim \frac{1}{v^3} - \frac{1}{2} + \frac{1}{24}v^3 \quad \text{as } v \to 0, \tag{A 7}$$

a simple application of (A 1) indicates that

$$Z_I(\xi, t) \sim \xi - \frac{2}{3\xi^5} \quad \text{as } \xi \to \infty. \tag{A 8}$$

However, in this case we must take care to include the contribution due to the point of stationary phase, and hence arrive at the final approximation, (3.24).

Analysis of the full linearized solution for the cone when $r = O(1)$ and $t \ll 1$

Using (3.29) we can show that

$$Z(r,t) - r \sim \frac{t^2}{2\pi\mathrm{i}} \int_{c-\mathrm{i}\infty}^{c+\mathrm{i}\infty} \frac{\mathrm{e}^\sigma}{\sigma} \int_0^\infty v J_0(vr) \frac{1}{\sigma^2 + 4\sigma v^2 t - 4v^3\sigma^{1/2}t^{3/2}} \mathrm{d}v\, \mathrm{d}\sigma$$
$$\text{for } r = O(1) \text{ as } t \to 0. \tag{A 9}$$

It is now instructive to note that

$$H_0\left[\frac{1}{v^2 + \frac{1}{4}\sigma t^{-1}}\right] = K_0\left(\frac{r}{2t^{1/2}}\sigma^{1/2}\right). \tag{A 10}$$

This means that, if we simply neglect the term $4v^3\sigma^{1/2}t^{3/2}$ in the denominator of the integrand in (A 9), we obtain an exponentially small contribution, provided $r \gg t^{1/2}$. This is consistent with the fact that the expansion of the argument of the Hankel transform in (A 10) for $t \ll 1$ consists of positive even powers of v only. We must therefore include the term $4v^3\sigma^{1/2}t^{3/2}$ in the denominator of the integrand in (A 9) in order to pick up the algebraic behaviour of the deformation of the interface. Since

$$\frac{1}{\sigma^2 + 4\sigma v^2 t - 4v^3\sigma^{1/2}t^{3/2}} \sim \frac{1}{\sigma^2}\left(1 - \frac{4t}{\sigma}v^2 + \frac{4t^{3/2}}{\sigma^{3/2}}v^3\right) \quad \text{as } t \to 0, \tag{A 11}$$

a simple application of (A 1) leads to the asymptotic approximation (3.28).

REFERENCES

Billingham, J. & King, A. C. 1995 The interaction of a moving fluid/fluid interface with a flat plate. *J. Fluid Mech.* **296**, 325.

Chen, Y.-J. & Steen, P. H. 1997 Dynamics of inviscid capillary breakup: collapse and pinchoff of a film bridge. *J. Fluid Mech.* **341**, 245.

Day, R. F., Hinch, E. J. & Lister, J. R. 1998 Self-similar capillary pinchoff of an inviscid fluid. *Phys. Rev. Lett.* **80**, 704.

Decent, S. P. & King, A. C. 1999 Surface tension driven flow in a slender cone. *In preparation.*

Eggers, J. 1997 Nonlinear dynamics and breakup of free surface flows. *Rev. Mod. Phys.* **69**, 865.

Gradshteyn, I. S. & Ryzhik, I. M. 1994 *Tables of Integrals, Series and Products, 5th Edn.* Academic.

Keller, J. B., King, A. C. & Ting, L. 1995 Blob formation. *Phys. Fluids* **7**, 226.

Keller, J. B. & Miksis, M. J. 1983 Surface tension driven flows. *SIAM J. Appl. Maths* **43**, 268.

King, A. C., Billingham, J. & Popple, D. F. 1999 On the interaction between an advected fluid/fluid interface and a flat plate. *Q. J. Math. Mech.* **52**, 453–468.

Lighthill, M. J. 1958 *Fourier Analysis and Generalised Functions.* Cambridge University Press.

Lister, J. R. & Stone, H. A. 1998 Capillary breakup of a viscous thread surrounded by another viscous fluid. *Phys. Fluids* **10**, 2758.

Misra, O. P. & Lavoine, J. L 1986 *Transform Analysis of Generalized Functions.* North-Holland.

Peregrine, D. H., Shoker, G. & Symon, A. 1990 The bifurcation of liquid bridges. *J. Fluid Mech.* **212**, 25.